Central European Journal of Energetic Materials
ISSN 1733-7178; e-ISSN 2353-1843

Cent. Eur. J. Energ. Mater. 2018, *15*(1): 3-17; (**These page numbers will be altered**);
DOI: 10.22211/cejem/81604

Application of BCHMX in Shaped Charges against RHA Targets Compared to Different Nitramine Explosives

Ahmed Elbeih,[1*] Tamer Elshenawy,[2] Svatopluk Zeman,[3] Zbynek Akstein[4]

[1] *Military Technical College, Kobry Elkobbah, 11765 Cairo, Egypt*
[2] *Technical Research Center, Cairo, Egypt*
[3] *University of Pardubice, Czech Republic*
[4] *Explosia Company, Czech Republic*
[*] *E-mail: elbeih.czech@gmail.com*

Abstract: In this work, a new bicyclic nitramine, *cis*-1,3,4,6-tetranitrooctahydroimidazo-[4,5-d]imidazole (bicyclo-HMX or BCHMX), has been tested for its performance as a shaped charge explosive filler in comparison with three other interesting cyclic nitramines. Four shaped charges were prepared using different nitramine-based plastic bonded explosives (PBXs), and their performance was measured experimentally in terms of the penetration depth into laminated rolled homogeneous armour (RHA) targets. The explosive fillers were highly pressed PBXs based on RDX, HMX, BCHMX and CL-20, bonded by Viton A binder. The Autodyn numerical hydrocode was implemented to determine the shaped charge jet's characteristics and its penetration depth. The experimental and calculated detonation characteristics of the explosives used are reported. Relationships between the detonation characteristics of the explosives and the jet characteristics were observed. The results show that CL-20 is the most powerful explosive, with the largest penetration depth into the RHA target, while BCHMX explosive has a relatively enhanced penetration depth with respect to RDX explosive. The results of the Autodyn code calculations are consistent with the experimental measurements, with a maximum difference of 6.6%.

Keywords: BCHMX, shaped charge, jet penetration, nitramines

1 Introduction

A shaped charge jet has an excellent penetration capability into various targets. Thus, it has been successfully used in both military and civilian applications. Theoretically, explosives with high performance produce faster jets, great kinetic energy and deep penetration [1]. The energy obtained from the high explosive during its detonation is related to the Gurney energy of the explosive, which is the energy liberated from the high explosive and transformed into mechanical work imparted to the liner element. Increasing the Gurney energy leads to an increase in the collapse velocity of the liner element, and therefore the jet velocity will be improved. As a result, the jet kinetic energy and its penetration potential into the target will be enhanced. The loading density of the explosives also affects the penetration depth of the shaped charges into the target materials. The explosive should be pressed under vacuum to remove air bubbles and to increase its density, as presented by Renfre *et al*. [2]. Moreover, the shaped charges used for military purposes should be tested by flash X-ray in order to check for air voids and cracks. Other parameters such as the grain size and homogeneity of the high explosives should also be considered [1]. It has been claimed that shaped charge warheads might perform much more efficiently when the explosive filler has a particle size of less than 200 μm [3].

Several studies have investigated the effects of explosive type [4, 5], explosive particle size [6-8], binder system [9-12], and their physical or/and chemical compatibility [13, 14] on the energetic performance of plastic bonded explosives. Plastic bonded explosives (PBXs) containing ε-HNIW (2,4,6,8,10,12-hexanitro-2,4,6,8,10,12-hexaazaisowurtzitane, ε-CL-20) have been intensively investigated, since it has an excellent explosive performance [15, 16], high energy density, and good thermal stability [13]. PBX compositions based on octahydro-l,3,5,7-tetranitro-1,3,5,7-tetrazocine (HMX), and ε-HNIW (2,4,6,8,10,12-hexanitro-2,4,6,8,10,12-hexaazaisowurtzitane, ε-CL-20) tend to be significantly more expensive than conventional ones based on hexahydro-l,3,5-trinitro-1,3,5-triazine (RDX). A relatively new explosive, *cis*-1,3,4,6-tetranitro-octahydroimidazo-[4,5-d]imidazole (bicyclo-HMX or BCHMX) [17-20], which may become a useful and cost effective alternative to HMX and ε-HNIW, has been introduced.

The main goal of the present research was to determine the usability of the new BCHMX as a plastic bonded explosive and compare its performance to other powerful nitramine-based PBXs (RDX, HMX, CL-20) using small caliber shaped charges filled with the specified PBXs. A measure of the explosive performance is presented in terms of the jet penetration depth into RHA targets. In addition,

the Autodyn hydrocode has been used to determine the jet's characteristics and its penetration potential using various explosive charges.

2 Experimental

The small caliber liners used in this study were made from electrolytic oxygen-free copper with a purity of 99.99% Cu, which has good machinability and ductility, with a uniform liner wall thickness of 1.2 mm, as illustrated in Figure 1. The liner had a base diameter of 31.8 mm, cone angle of 50°, and height of 27.35 mm, and was produced from an initial copper sheet thickness of 3 mm by metal-stamping with attenuation of the wall. The copper liners were obtained from Explosia Co., Pardubice, CZ. The metallographic structure of the produced liners exhibited a grain size: 15-25 μm and hardness 55-65 HV5. The charge case was manufactured from a polyethylene cylindrical bar using a CNC machine. The case had an external diameter of 34 mm, and an internal wall thickness of ~2.0 mm. The four different types of plastic bonded explosives (PBXs) were based on 95 wt.% of the individual explosive bonded by 5% Viton A 200 [8].

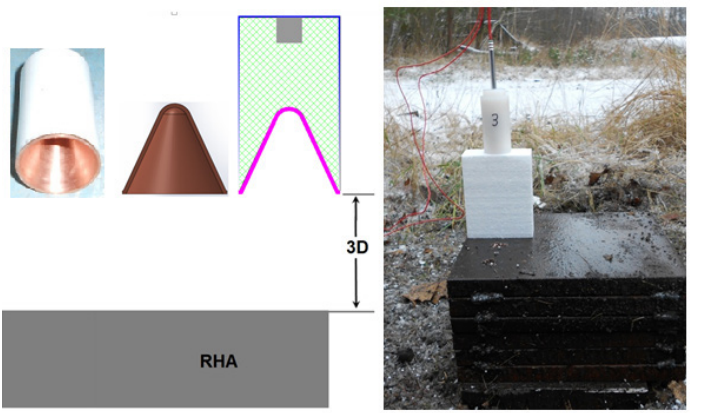

Figure 1. A sketch of the shaped charge assembly and the experimental arrangement

The pure explosive fillers were RDX, BCHMX, HMX and CL-20. The prepared samples were designated as RDX-V5, BCHMX-V5, HMX-V5 and CL-20-V5, of masses 62.3 *g*, 64 *g*, 65.2 *g* and 69 g, respectively. The detonation velocities of the prepared samples were measured experimentally and the main detonation characteristics were further calculated using computer code EXPLO5 [21]

as reported in Ref. [8]. The charges were pressed at a high specific pressing pressure of 486 MPa for 10 s, and were then placed in the PVC cylinder casing. A detonator no. 8 was used to initiate the four shaped charges as shown in Figure 1. The pressed explosive charges with the liner were placed inside the polyvinyl chloride (PVC) cylinder where all of the charges were kept at a distance of 96 mm (*i.e*. 3D; 3 times the caliber). The four shaped charges were fired against 8 laminated layers of a rolled homogeneous armour (RHA) target of 1 inch layer thickness.

3 Numerical modelling

Three different simulation schemes in Autodyn were used in the simulations, *i.e*.

a. The jetting analysis based on the unsteady state PER theory [22] was used to calculate the jet and slug velocities and masses. The outputs from this algorithm are the liner element collapse, flow and jet velocities, the liner collapse and deflection angles, as well as the jet kinetic energy and momentum.
b. The jet formation was simulated using the Euler method based on continuum mechanics in order to obtain the jet profile at different times. When the high explosive is detonated, the detonation wave sweeps the liner, collapsing it to form the jet and the slug. The formed jet and slug flow over the Euler meshes with a non-uniform velocity distribution towards the target. The output of this scheme was used as the input of the Lagrange-Lagrange interaction scheme.
c. The jet interaction (penetration) with the RHA target was simulated using the Lagrange method. In this scheme, the jet obtained from the jet formation Euler solver is remapped to the Lagrange moving grids and impacts the RHA target. The overall crater profile inside the RHA target is monitored. Further details, such as the erosion strain effect and mesh sensitivity analysis, as well as the validity and verification of this hydrocode, may be found in Ref. [23].

3.1 Material model

In jet formation, PER based jetting analysis and penetration simulations, relevant material models and parameters were established in Autodyn, which is briefly introduced for all of the numerical models for the liner, the explosive, the casing and the target materials separately.

3.1.1 The explosive charge

The equation of state (EOS) for the high explosive was the "Jones-Wilkins-Lee" (JWL) equation [24], *i.e.*

$$p = \mathrm{A}\left(1 - \frac{\omega V}{\mathrm{r}_1}\right) e^{-\frac{\mathrm{r}_1}{V}} + \mathrm{B}\left(1 - \frac{\omega V}{\mathrm{r}_2}\right) e^{\frac{-\mathrm{r}_2}{V}} + \omega V E \qquad (1)$$

where p is the pressure, V is the relative volume and equal to $\frac{volume\ undetonated\ explosive}{volume\ of\ detonation\ products} = \frac{\rho}{\rho_0}$, (as the mass is fixed, so the relative volume could be represented as relative densities), is the reference density, ρ the current density, and A, B, r_1, r_2 and ω are constants [25]. E is the specific internal energy per unit mass. These constants are chosen to satisfy the following conditions: the measured Chapman-Jouguet (C-J) state, the measured expansion behaviour in the cylinder test, thermodynamic limitations at large expansions, and hydrodynamic continuity [2]. The values of the experimental constants for some explosives have been determined from sideways plate push dynamic test experiments [26] and cylinder expansion tests [27-29]. The values of the above mentioned constants were calculated from the Mat Lab Simulink program based on intensive calculations considering various densities and the relevant detonation pressure values, and hence the optimized JWL equation of state parameters were estimated analytically and are listed in Table 1 for the explosive materials studied.

Table 1. The JWL parameters for the explosive charges studied

	RDX-V5	BCHMX-V5	HMX-V5	CL-20-V5
Reference density [g/cm^3]	1.76	1.81	1.84	1.95
Parameter A [kPa]	7.50×10^8	3.97×10^8	5.02×10^8	1.64×10^9
Parameter B [kPa]	7.60×10^7	1.71×10^7	7.92×10^7	1.86×10^8
Parameter r_1 (none)	3.84	4.07	4.28	6.50
Parameter r_2 (none)	1.26	0.98	1.11	2.70
Parameter ω (none)	0.47	0.37	0.28	0.55
C-J detonation velocity [m/s] [8]	8424	8612	8730	9194
C-J energy/unit volume [kJ/m^3]	1.01×10^7	1.11×10^7	1.07×10^7	1.20×10^7
C-J Pressure [kPa] [8]	3.02×10^7	3.30×10^7	3.35×10^7	3.81×10^7

3.1.2 The copper liner

The EOS of the copper liner material is the shock model and its strength model is neglected for the extremely large pressure on the liner walls during liner

collapse. It has been shown experimentally that for most solids and liquids that do not undergo a phase change, the values of shock velocity (U) and material velocity behind the shock (Up) on the shock Hugoniot can be adequately fitted to a straight line. This is valid up to shock velocities around twice the initial speed of sound C_0 and shock pressures of the order of 100 GPa [29]; *i.e.*

$$U = C_0 + sU_p \tag{2}$$

where s is a material constant that represents the slope of the shock velocity-particle velocity relationship. The Mie-Gruneisen EOS based on the shock Hugoniot is expressed as:

$$p = p_H + \Gamma\rho(e - e_H) \tag{3}$$

where Γ is the Gruneisen Gamma coefficient and is equal to $B_0/(1 + \mu)$ where B_0 is a constant, $\Gamma\rho = \Gamma_0\rho_0$ = constant is assumed; ρ is the density. p_H and e_H are the Hugoniot pressure and energy, respectively, given by:

$$p_H = \frac{\rho_o c_o^2 \mu(1+\mu)}{[1-(s-1)\mu]^2} \tag{4}$$

and

$$e_H = \frac{1}{2}\frac{p_H}{\rho_o}\left(\frac{\mu}{1+\mu}\right) \tag{5}$$

where $\mu = (\rho/\rho_0) - 1$ is the compressibility. The mechanical properties of the copper liner, casing material and the target are listed in Table 2 based on the shock equation of state and at the reference temperature 300 K, where the constants in the previous equations were taken from the material library.

Table 2. The mechanical properties of the liner and casing materials [29]

Parameter	Copper	Polyethylene	RHA Target
Reference density [g/cm^3]	8.93	0.915	7.86
Gruneisen coefficient	2.02	1.64	1.67
Parameter C [m/s]	3940	2901	4610
Parameter S (none)	1.489	1.481	1.73

3.1.3 The charge cases

The material used for the charge case was polyethylene with the shock EOS, which has been described previously for the liner material, while its strength model was neglected. The parameters for the shock EOS for the polyethylene charge casing material is listed in Table 2.

3.1.4 Rolled Homogeneous Armour (RHA) target

The EOS of the RHA target material is the shock model without strength model. The behavior of the target material during the penetration of the shaped charge jet is considered in a fully hydrodynamic regime. The shock equation of state parameters of the target material is explained in section 3.1.2; all of the parameters of the shock EOS are listed in Table 2.

4 Results and Discussion

4.1 Shaped charge jetting analysis and penetration calculations summary

Elshenawy *et al*. presented a numerical model to estimate the virtual origin of a shaped charge jet in order to determine the effective standoff distance from the target surface [30]. The jet formation numerical simulations show the stretching of the copper jet during liner collapse until it reaches the target surface at the designated stand-off distance (*i.e*. 3 times its calibre). A sample of the modelled shaped charge liner collapse and jet formation using the RDX-V5 explosive charge is shown in Figure 2, which includes the velocity contours during and after jet formation for the same explosive charge. The velocity contours show the liner collapsing and the beginning of the jet formation at 8.1 μs, after which the jet begins to stretch with a velocity gradient at the tip of around 6230 m/s and its slug of around 1248 m/s. Figure 3 shows the initial setup of the numerical Lagrangian jet against the RHA Lagrangian target just before the start of hydrodynamic penetration.

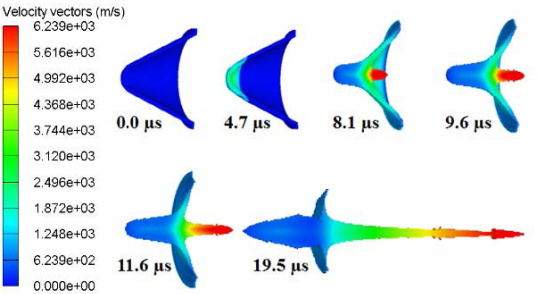

Figure 2. `The absolute velocity contours of jet formation at different times from the detonation moment using an RDX explosive charge

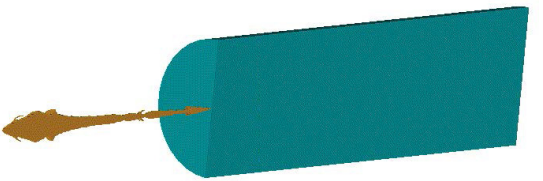

Figure 3. The resultant shaped charge jet from the explosive charge facing the RHA target

A summary of the jetting analysis data of the four charges is shown in Figure 4, which is considered a finger print for a specific shaped charge. This figure shows a considerable difference between the four curves in their collapse velocity, especially near the apex region where the tip forms. The direct explicit relation between the collapse velocity V_0, the stagnation velocity V_1, the flow velocity V_2 and the jet tip velocity V_j can be obtained from the unsteady state PER theory [22]. The collapse velocity, which has a direct impact on the jet tip velocity and its mass, depends on the energy liberated from the explosive material in contact with the liner material. Since CL-20 has the highest detonation velocity and detonation heat, it showed a 27.3% increase in the collapse velocity relative to the RDX-V5 charge. On the other hand, the BCHMX-V5 charge showed only a 1.6% increase in the maximum collapse velocity relative to the RDX-V5 charge. The remarkable difference between the collapse velocities for the four charges is the main reason why there is a quite large difference in their jet tip velocities, which in turn governs the penetration depth as confirmed in the actual experiments. Table 3 summarizes the main jetting characteristics obtained by the numerical analysis, together with the detonation characteristics of the four explosive charges used, while Figure 5 shows the relation between

the maximum collapse velocities as a function of the detonation velocity of the explosive charge used. An interesting linear relationship is observed, which confirms that an explosive with a higher detonation velocity generates a higher collapse velocity.

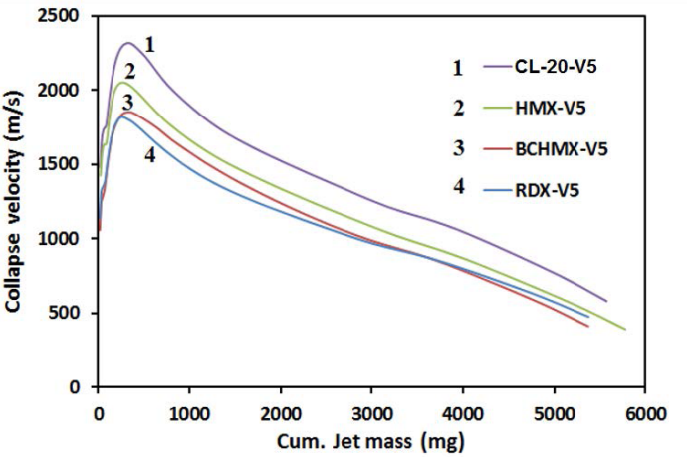

Figure 4. Collapse velocity *vs*. the cumulative jet mass, calculated from the Autodyn numerical jetting analysis

Table 3. Dependence of the jet characteristics on the explosive charge type

Explosive material	RDX-V5	BCHMX-V5	HMX-V5	CL-20-V5
Liner mass [g]	18.6	18.6	18.6	18.6
Detonation velocity [m/s] [8]	8424	8612	8730	9194
Gurney velocity* $\sqrt{2E}$ [m/s]	2735	2796	2834	2985
Jet mass [g]	5.37	5.37	5.78	5.57
Jet mass to liner [%]	28.87	28.87	31.08	29.94
Jet tip velocity [m/s]	6230	6308	6763	7419
Maximum collapse velocity [m/s]	1819	1849	2052	2316

* $\sqrt{2E}$ is calculated from the empirical relation in Ref. [31]

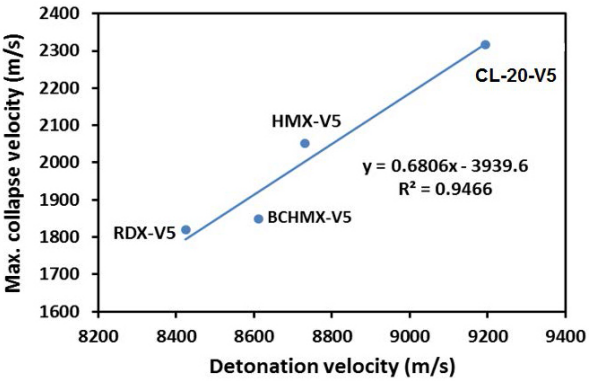

Figure 5. The maximum collapse velocity obtained as a function of the VOD of the explosive used

Based on the standard jetting analysis for the four explosive charges and the relevant numerical and experimental penetration tests, Table 4 summarizes the net kinetic energy of the four jets produced and the relevant penetration depths. Amazingly the increase in the jet kinetic energy from the CL-20-V5 explosive charge, with respect to the RDX-V5 explosive charge, was found to be 60% compared to a mild increase of 7% in the case of the BCHMX-V5 explosive charge. Results of the penetration depths are consistent with the theoretical calculations of the jet kinetic energy, which showed a significant difference in the penetration depths between the CL-20-V5 and the BCHMX-V5 charges (2.6 cm, *i.e.* about 20% increase). The effect of the kinetic energy of the shaped charge jet on its penetration capability is discussed in Ref. [32].

It is not only the explosive type that influences the jet velocity and its penetration depth; its loading density also has a considerable effect. The RDX-V5 charge has the lowest loading density of the four charges studied (1.76 g/cm^3), which has a direct impact on its detonation characteristics, especially the detonation velocity, which was found to be the lowest at 8424 m/s, as measured in [8], and therefore exhibited the lowest jet tip velocity. On the other hand, the CL-20-V5 charge had the largest loading density of 1.95 g/cm^3 and showed the most powerful penetration potential. This explosive produced a jet tip velocity of 7419 m/s and a jet mass ratio of 29.94%.

This result was confirmed by the experimental measurements, where the shaped charge filled with CL-20-V5 produced the largest penetration depth of 15.36 cm into the RHA, as indicated in Figure 6.

Table 4. Effect of the jet kinetic energy (K.E.) on the penetration depth of the four explosive charges

Explosive material	RDX-V5	BCHMX-V5	HMX-V5	CL-20-V5
Jet K.E. [kJ]	16.6	17.8	20.5	26.5
Jet K.E. relative to K.E. of RDX	1	1.07	1.23	1.60
Penetration; Numerical [cm]	12.1	13.0	13.5	14.7
Penetration; Experiment [cm]	11.4	12.8	13.9	15.4
$(P_{EXP.}-P_{Num})/P_{EXP.}\times 100$ [%]	−6.6	−1.9	2.8	4.3

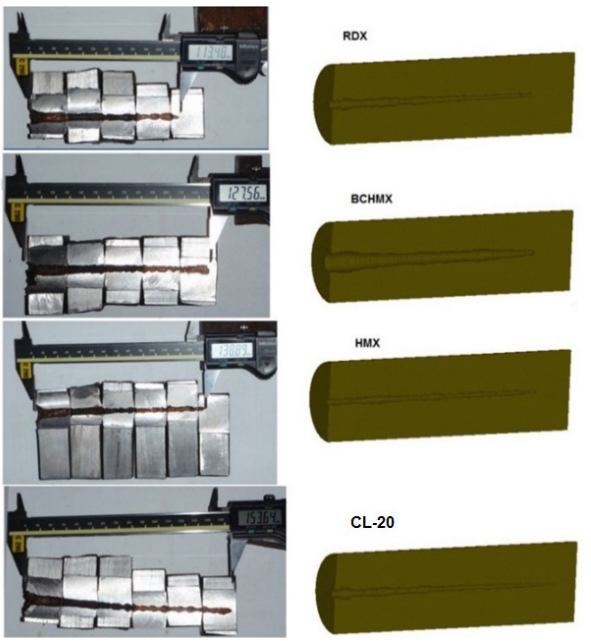

Figure 6. The crater profile along the penetrated RHA (left) and the numerical Autodyn penetration (right) for the four different explosive charges

Three linear relationships were obtained between both the penetration depth and the jet tip velocity and (ρD^2), as shown in Figure 7. Both the experimental and numerical penetration have similar direct relations with the (ρD^2) values; but their slopes are somewhat different due to the numerical approximation governing parameters such as erosion strain, mesh separation and the selected material models of the RHA and the copper jet. On the other hand, a linear relation between the jet tip velocity and ρD^2 values was also observed, which confirms the dependence of the jet tip velocity on the detonation pressure, represented here by ρD^2.

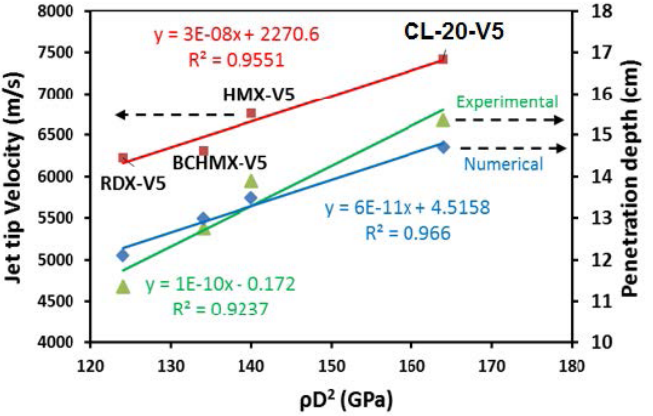

Figure 7. The derived relations between both the jet tip velocity and the penetration depth with (ρD^2)

5 Conclusions

BCHMX has been implemented successfully as a shaped charge PBX explosive filler and compared to three other nitramines. The characteristics of the different explosive mixtures have been theoretically obtained using Explo5 software, which have then been used to estimate the jetting data for the four pressed nitramine PBXs. Significant differences in the kinetic energy of their jets were obtained, with 7%, 23% and 60% increases for BCHMX-V5, HMX-V5 and CL-20-V5 respectively, compared to that of the RDX-V5 baseline charge. The variation in the K.E. of these jets exhibited a remarkable variation in their penetration potential into the RHA, which was related linearly with the detonation pressure (represented by ρD^2).

It was also concluded that the BCHMX5-V charge exhibited a 12.4% increase in penetration depth into the RHA laminated target compared to the RDX-V5 charge, while the HMX-V5 charge had a 22.4% increase in its penetration capability relative to the RDX-V5 baseline charge. The highly brisant CL-20-V5 explosive charge achieved a 35% increase in the penetration depth compared with the RDX-V5 charge.

The calculated results using the Autodyn hydro-code were found to be consistent with the experimental measurements, with only 6.6% maximum difference in the numerical penetration depth.

References

[1] Walters, P.; Zukas, J. *Fundamentals of Shaped Charge*. Wiley Interscience Publication, New York, USA **1989**; ISBN 9780471621720.

[2] Renfre, S.; Locks, W. *Conn, Liner and Improved Shaped Charge Especially for Use in a Well Pipe Perforating Gun*. Patent US 5509356A, **1996**.

[3] Elwany, H. *The Use of Polymer Bonded Explosives in Improved Linear Shaped Charge Designs*. PhD dissertation, Cranfield University, UK **1994**.

[4] Elbeih, A.; Wafy, T. Z.; Elshenawy, T. Performance and Detonation Characteristics of Polyurethane Matrix Bonded Attractive Nitramines. *Cent. Eur. J. Energ. Mater.* **2017**, *14*(1): 77-89.

[5] Elbeih, A.; Zeman, S. Characteristics of Melt Cast Compositions Based on *cis*-1,3,4,6-Tetranitrooctahydroimidazo-[4,5 d]imidazole (BCHMX)/TNT. *Cent. Eur. J. Energ. Mater.* **2014**, *11*(4): 487-499.

[6] Willey, T.; Lauderbach, L.; Gagliardi, F.; Buuren, F.; Glascoe, E.; Tringe, J.; Lee, J.; Springer, K.; Ilavsky, J. Mesoscale Evolution of Voids and Microstructural Changes in HMX-Based Explosives During Heating through the β-δ Phase Transition. *J. Appl. Phys.* **2015**, *118*(5): 055901.

[7] Elbeih, A.; Zeman, S.; Pachmáň, J. Effect of Polar Plasticizers on the Characteristics of Selected Cyclic Nitramines. *Cent. Eur. J. Energ. Mater.* **2013**, *10*(3): 339.

[8] Elbeih, A.; Zeman, S.; Pachmáň, J.; Vávra, P.; Trzciński, W.; Suceska, M.; Akstein, Z. Study of Plastic Explosives Based on Attractive Cyclic Nitramines. Part II. Detonation Characteristics of Explosives with Polyfluorinated Binders. *Propellants Explos. Pyrotech.* **2013**, *38*(2): 238-243.

[9] Thompson, D.; Deluca, R.; Archuleta, J.; Brown, G.; Koby, J. Taylor Impact Tests on PBX Composites: Imaging and Analysis. *J. Phys.: Conf. Ser.* **2014**, *500*: 112062.

[10] Elbeih, A.; Zeman, S.; Jungova, M.; Akstein, Z. Effect of Different Polymeric Matrices on Sensitivity and Performance of Interesting Cyclic Nitramines. *Cent. Eur. J. Energ. Mater.* **2012**, *9(*2): 17.

[11] Agrawal, J. *High Energy Materials: Propellants, Explosives and Pyrotechnics*. John Wiley & Sons, **2010**; ISBN 978-3-527-32610-5.

[12] Hussein, A. K.; Elbeih, A.; Zeman, S. Thermo-analytical Study of *cis*-1,3,4,6-Tetranitrooctahydroimidazo-[4,5-d]imidazole (BCHMX) and 1,1-Diamino-2,2-dinitroethene (FOX-7) in Comparison with a Plastic Bonded Explosive Based on Their Mixture. *J. Anal. Appl. Pyrolysis* **2017**, *128*: 304-313.

[13] Zeman, S.; Elbeih, A.; Yan, Q.-L. Notes on the Use of the Vacuum Stability Test in the Study of Initiation Reactivity of Attractive Cyclic Nitramines in the C4 Matrix. *J. Therm. Anal. Calorim.* **2013**, *112*(3): 1433-1437.

[14] Yan, Q.-L.; Zeman, S.; Elbeih, A.; Akstein, Z. The Influence of the Semtex Matrix on the Thermal Behavior and Decomposition Kinetics of Cyclic Nitramines. *Cent. Eur. J. Energ. Mater.* **2013**, *10*(4): 509-528.

[15] Elbeih, A.; Mohamed, M.; Wafy, T. Z. Sensitivity and Detonation Characteristics of Selected Nitramines Bonded by Sylgard Binder. *Propellants Explos. Pyrotech.*

2016, *41(*6): 1044-1049.

[16] Yan, Q.-L.; Zeman, S.; Sanchez, J. P. E.; Zhang, T.-L.; Perez-Maqueda, L. A.; Elbeih, A. The Mitigation Effect of Synthetic Polymers on Initiation Reactivity of CL-20: Physical Models and Chemical Pathways of Thermolysis. *J. Phys. Chem. C*. **2014**, *118*(40): 22881-22895.

[17] Klasovity, D.; Zeman, S.; Růžicka, A.; Jungova, M.; Rohac, M. *cis*-1,3,4,6-Tetranitrooctahydroimidazo-[4,5-d]imidazole (BCHMX), Its Properties and Initiation Reactivity. *J. Hazard. Mater.* **2009**, *164*: 954-961.

[18] Elbeih, A.; Abd-elghany, M.; Klapotke, T. M. Kinetic Parameters of PBX Based on *cis*-1,3,4,6-Tetranitrooctahydroimidazo-[4,5-d]imidazole Obtained by Isoconversional Methods Using Different Thermal Analysis Techniques. *Propellants Explos. Pyrotech.* **2017**, *42*(5): 268-276.

[19] Elbeih, A.; Elshenawy, T.; Gobara, M. Application of cis-1,3,4,6-Tetranitrooctahydroimidazo-[4,5d]imidazole (BCHMX) in EPX-1 Explosive. *Def. Sci. J.* **2016**, *66*(5): 499-503.

[20] Hussein, A. K.; Elbeih, A.; Zeman, S. Thermal Decomposition Kinetics and Explosive Properties of a Mixture Based on *cis*-1,3,4,6-Tetranitrooctahydroimidazo-[4,5-d]imidazole and 3-Nitro-1,2,4-triazol-5-one (BCHMX/NTO). *Thermochim. Acta* **2017**, *655*: 292-301.

[21] Sućeska, M. Calculation of Detonation Parameters by EXPLO5 Computer Program. In: *Explosion, Shock Wave and Hypervelocity Phenomena in Materials*; ISBN 978-087849-950-2. Periodical: *Mater. Sci. Forum* **2004**, *465*: 325.

[22] Pugh, E.; Eichelberger, R.; Rostoker, N. Theory of Jet Formation by Charges with Lined Conical Cavities. *J. Appl. Phys.* **1952**, *23*(5): 532-536.

[23] Elshenawy, T.; Elbeih, A.; Li, Q. M. A Modified Penetration Model for Copper Tungsten Shaped Charge Jets with Non-uniform Density Distribution. *Cent. Eur. J. Energ. Mater.* **2016**, *13*(4): 927-943.

[24] Baudin, G.; Serradeill, R. Review of Jones-Wilkins-Lee Equation of State. *EPJ Web of Conferences*, **2010**, *10*: 21; DOI: 10.1051/epjconf/20101000021.

[25] Lee, E.; Hornig, H.; Kury, J. *Adiabatic Expansion of High Explosive Detonation Products*. Technical Report UCRL--50422, Lawrence Radiation Lab., California Univ., Livermore **1968**.

[26] Tarver, C.; Tao, W.; Lee, C. Sideways Plate Push Test for Detonating Solid Explosives. *Propellants Explos. Pyrotech.* **1996**, *21*(5): 238-246.

[27] Elek, P.; Dzingalasevic, V.; Jaramaz, S.; Mickovic, M. Determination of Detonation Products Equation of State from Cylinder Test: Analytical Model and Numerical Analysis. *Thermal Science* **2015**, *19*(1): 35-48.

[28] Kato, H.; Kaga, N.; Takizuka, M.; Hamashima, H.; Itoh, S. Research on the JWL Parameters of Several Kinds of Explosives. *Mater. Sci. Forum* **2004**, *465-466*: 271.

[29] *AUTODYN® Jetting Tutorial*, 3rd revision, Century Dynamics, USA **1997**.

[30] Elshenawy, T.; Elbeih, A.; Klapötke, T. M. A Numerical Method for the Determination of the Virtual Origin Point of Shaped Charge Jets Instead of Using Flash X-ray Radiography. *J. Energ. Mater.* DOI: 10.1080/07370652.2017.1324532.

[31] Koch, A.; Arnold, N.; Estermann, M. A Simple Relation between the Detonation Velocity of an Explosive and Its Gurney Energy. *Propellants Explos. Pyrotech.* **2002**, *27*: 365-368.
[32] Davinson, A.; Pratt, D. A Hydrocode-Designed Well Perforator with Exceptional Performance. *Int. Symp. Ballist. Proc. 17th*, Midrand, South Africa **1998**.